Geophysical Research Letters

RESEARCH LETTER

10.1029/2018GL080689

Key Points:

- Central Pacific ENSO has higher percentage occurrence during 1997–2007 period
- Phytoplankton biomass and Chl-a have similar physical mechanisms during EP and CP ENSO
- Agglomerative hierarchical (AHC) clustering technique allowed clear separation of the EP and CP ENSO

Supporting Information:

- Supporting Information S1

Correspondence to:
P. Sharma,
priyash@sas.upenn.edu

Citation:
Sharma, P., Singh, A., Marinov, I., & Kostadinov, T. (2019). Contrasting ENSO types with satellite derived ocean phytoplankton biomass in the Tropical Pacific. *Geophysical Research Letters*, *46*. https://doi.org/10.1029/2018GL080689

Received 29 SEP 2018
Accepted 9 MAY 2019
Accepted article online 7 JUN 2019

Contrasting ENSO Types With Satellite-Derived Ocean Phytoplankton Biomass in the Tropical Pacific

Priya Sharma[1,2], A. Singh[2], I. Marinov[1], and T. Kostadinov[3]

[1]Department of Earth and Environmental Science, University of Pennsylvania, Philadelphia, PA, USA, [2]Pacific Center for Environment and Sustainable Development, The University of the South Pacific, Suva, Fiji, [3]Department of Liberal Studies, California State University, San Marcos, CA, USA

Abstract Observed variations in the tropical phytoplankton community structure and biogeochemical processes have been linked to the El Niño Southern Oscillation, a driver of large-scale natural climate variability on interannual timescales. Satellite bio-optical algorithms have allowed us to derive complex biological parameters from the surface ocean via remote sensing, providing a scientific platform to investigate biological relationships with climate indices. Studies have focused in-depth on contrasting types of the ENSO types with various physical parameters with only a few recent studies focusing on satellite-observed chlorophyll-a, with however none focusing on phytoplankton biomass itself. Here we review the types of ENSO and its effect on backscattering-based biomass using different statistical techniques, over the 1997-2007 period. We also contrast the responses of phytoplankton biomass with those of chlorophyll-a and their physical drivers in various types of ENSO. Signatures of various ENSO types are observed in the physical and biological fields.

1. Introduction

Phytoplankton are microscopic cellular organisms omnipresent in the surface ocean. The photosynthetic activity of phytoplankton is the level one of the marine food chains and supports trophic web. Moreover, phytoplankton affect the water column's optical properties via light absorption and backscattering (Mobley et al., 2002; Stramski & Kiefer, 1991), which allows for their detection via passive ocean-color remote sensing (Gordon & Morel, 1983; Sathyendranath & Platt, 1989). Remote sensing is a reliable tool (in addition to in situ data) for gathering observational data on spatio-temporal scales to characterize the structure and function of global marine ecosystems and to achieve predictive understanding. Phytoplankton adjusts its pigment composition to changes in environmental conditions such as light. Consequently, chlorophyll-a (Chl-a) may not be the best indicator for phytoplankton community structure and abundance. Therefore, we need independent estimates for phytoplankton biomass. Bio-optical algorithms have previously been applied to detect phytoplankton biomass separately from Chl-a (Behrenfeld et al., 2005; Kostadinov et al., 2009, 2010, 2016). Results from recent studies show that variations in ocean biogeochemical processes in the tropics are linked to the El Niño Southern Oscillation (ENSO) phenomenon (Gierach et al., 2012; Radenac et al., 2012).

ENSO phenomenon oscillates between a warm (El Niño) and a cold (La Niña [LN]) phase. Tropical-extratropical interactions, atmospheric pressure teleconnections, and ocean-atmosphere feedback stimulate anomalous variations in trade wind strength and sea surface temperature (SST). The evolution of ENSO events is well documented since the past two decades (Wang & Weisberg, 2000). The scientific literature has been well established on the different types of El Niño and their characteristics that contrast the classic Eastern Pacific El Niño (EPEN). El Niño Modoki (Ashok et al., 2007) is one of the recent El Niño types that have been discovered with multiple nomenclatures, such as the “Warm-Pool El Niño” (Kug et al., 2009) “Central Pacific El Niño” (CPEN; Kao & Yu, 2009), or “Dateline El Niño” (Larkin & Harrison, 2005a, 2005b).

The maximum SST anomalies confined in the central-eastern equatorial and dominantly in the central equatorial tropical Pacific region contrast the EPEN and CPEN, respectively. Multiple studies have focused on distinguishing EPEN and CPEN using SST (Ashok et al., 2007), sea surface salinity (Ashok et al., 2007; Singh et al., 2011), precipitation (Feng & Li, 2011; Zhang et al., 2011), and subsurface temperature (Yu & Kim, 2010), while a couple of new studies discuss the impacts of EPEN and CPEN based on

satellite-derived Chl-a (Messié & Chavez, 2013; Radenac et al., 2012; Turk et al., 2011) and primary production (PP) and phytoplankton growth (Racault et al., 2016, 2017). However, no study has characterized different types of El Niño using backscattering-based phytoplankton biomass.

In this manuscript, we use novel backscattering-based phytoplankton biomass data to diagnose further and contrast El Niño types and their characteristics over the 1997-2007 period. For the first time, we also define a biological index for EPEN and CPEN. Section 2 of the manuscript describes the data sets and statistics utilized in the paper. Section 3 is a comparison of the Chl-a and phytoplankton biomass anomalies in the Pacific equatorial region. Section 4 contrasts the EPEN and CPEN signatures of biomass using different statistical techniques. In section 5, we document the likely mechanisms responsible for observed ENSO-related biomass variations. The main findings are summarized in section 6.

2. Data and Methodology

2.1. Data Sets

The monthly 9-km horizontally gridded biomass product derived from a backscattering-based algorithm (Kostadinov et al., 2009, 2010, 2016) is used and is available from https://doi.pangaea.de/10.1594/PANGAEA.859005. The backscattering spectral slope and the magnitude are used as the inputs to the algorithm to retrieve the parameters of an assumed power law particle size distribution (PSD). The volume concentrations for different plankton size classes are calculated, using the PSD and its assumed relationship with backscattering spectral slope and additional assumptions, such as that relative proportions of biovolume are roughly constant across size classes (Kostadinov et al., 2016). One of the strengths of the assumption is that the particles are less sensitive to the physiological variability (Kostadinov et al., 2016, 2017; Mouw et al., 2017). However, the particle size class includes all particle sizes. Then, the existing allometric relationships (Menden-Deuer & Lessard, 2000) are applied to convert the biovolumes to the total carbon concentrations. We also used 9-km Chl-a (OCI: R2014) maps for the SeaWiFS period 1997-2010. The magnitudes of Chl-a have changed slightly from the standard (STD) algorithm (R2010) processing to the OCI algorithm processing. Chl-a and biomass are expressed in mg/m^3.

Physical variables used are 10-m daily wind speed (Berrisford et al., 2011), OSCAR ocean currents (Bonjean & Lagerloef, 2002), TOA/TRITON isothermal depth ($Z_{20°C}$: depth of the 20°C; Michael J. McPhaden et al., 1998), and Hadley Centre Sea Ice and Sea Surface Temperature analysis version 1 (HadISST1) SST. Table S1 in the supporting information provides details on data sources and resolution. The Multivariate El Niño Index was acquired from the National Center of Atmospherics Research climate data portal at https://climatedataguide.ucar.edu/. Time series of EPEN and CPEN indices (N_{CT} and N_{WP}, respectively) were constructed as in Ren and Jin (2011) using the HadISST1 data set. The piecewise linear combination of the climate indices, Niño-3 and Niño-4, are used to construct the EPEN and CPEN indices with conditioned by the ENSO phase. All the spatial data sets were obtained for the tropical Pacific region [30°S-30°N, 120°E-70°W] over the 1997-2010 period.

2.2. Preprocessing and Statistical Techniques

Seven monthly maps (in 2008 and 2009) had less than 60% of the data available for biomass and Chl-a over the 1997-2010 period; therefore, we only analyze data for the 1997-2007 period that had 100% temporal coverage. For Chl-a, the possibility was to adapt the Radenac et al. (2012) method and temporally replace the monthly maps with Aqua-Moderate Resolution Imaging Spectroradiometer (MODIS) ocean color maps. However, there are no other satellite data available for biomass using specifically Kostadinov et al. (2009, 2010) algorithms to replace the missing maps in our biomass data. Daily data sets were converted to monthly resolution. The 9-km resolution Chl-a and biomass products were regridded on a 1° grid using two-dimensional convolution with a 12×12 top-hat averaging kernel (Kostadinov et al., 2017). Nearest neighbor linear extrapolation was applied to fill in the data gaps due to sparse clouds.

To obtain the interannual signal, all data sets were first detrended over their respective periods to remove any long-term variability. Anomalies were calculated with respect to 1998-2007 period as some data sets were available only from September 1997 by removing the mean monthly climatology. The anomalies were then filtered using 13-month Hanning-filter to remove any remaining high-frequency signals. Filtering was

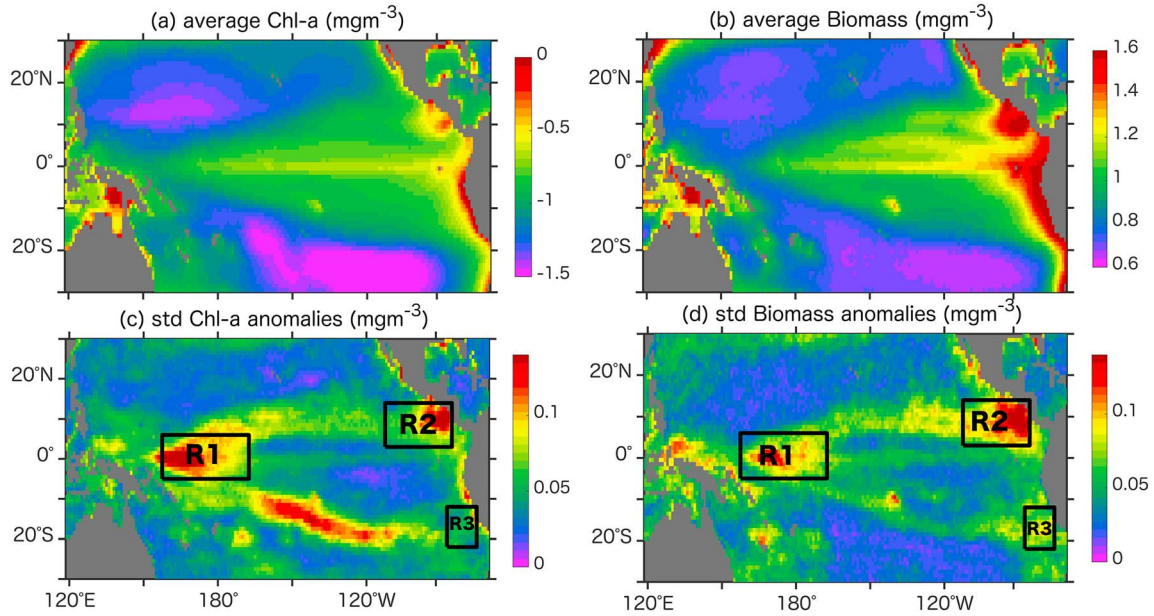

Figure 1. Mean and standard deviation maps for the (a and c) chlorophyll-a and (b and d) phytoplankton biomass for the September 1997 to December 2007 period. The three regions R1, R2, and R3 in black are regions with maximum variability chosen using Figure 1d.

performed on all the variables except Chl-a, as empirical orthogonal function (EOF) analysis on filtered and unfiltered Chl-a anomalies show similar ENSO patterns and loadings for the first three modes. This allowed for an additional 5 months of data at the beginning and end of the Chl-a time series. The Chl-a EOF patterns are consistent with Radenac et al. (2012) except for the magnitudes, which can be explained by the improved algorithms used to derive Chl-a. Biomass and Chl-a anomalies are lognormally distributed, as biological indices can span up to 3 orders of magnitude (Racault et al., 2016).

3. Chl-a and Biomass in the Equatorial Pacific Region

The 10-year mean phytoplankton biomass (Figure 1b) shows relatively low concentrations in the oligotrophic subtropical gyres ([Chl-a] <0.11 mg/m^3 (natural-log value of -0.96 mg/m^3; see Figure 1a), and comparatively high levels in the Central and South America ocean margins and the equatorial upwelling systems. The high biomass in these areas is due to the cold nutrient-rich water upwelled at the equatorial and coastal ocean surface waters supporting phytoplankton growth. Despite the nutrient concentration being high in the upwelling systems, the phytoplankton biomass is less than the time-averaged biomass concentration for the equatorial region (<1.2 mg/m^3, natural-log value) due to iron-limited and grazing maintaining (Lundry et al., 2003; Radenac et al., 2012). We observe robust biomass features near Papua New Guinea (PNG) and Solomon Islands coastal areas. Messié and Radenac (2006) suggest that elevated biomass concentrations are possibly due to the oceanic islands that deflect the deep ocean currents, flow, and wind circulation that allows horizontal advection and intermittent upwelling. The mean biomass pattern is similar to the mean Chl-a structure in Figure 1a and in Radenac et al. (2012); see their Figure 1): maxima in the tropical-tongue region and minima in the northern and southern subtropical gyres.

The interannual biomass variability (Figure 1d) mimics the Chl-a variability (Figure 1c; see Radenac et al., 2012, their Figure 1b) with maximum variability encompassed from the American coasts along curving trajectories toward 170°E at the equator. High variability is seen off the Californian coast and in the South American upwelling systems and around PNG and Solomon Islands. The interannual variability pattern for Chl-a is relatively higher and pronounced at the southern edge of the tropical tongue then biomass variability (Figure 1b). This variability is possibly due to the contraction and expansion of the tropical tongue/subtropical gyres during ENSO events.

4. ENSO Signatures of Biomass

4.1. EOF Analysis

An EOF analysis of logarithmic phytoplankton biomass anomalies (Figure S1a in the supporting information) shows that the first EOF mode explains 29.3% of the variance. The spatial structure exhibits negative loadings extending from the coast of California, along the Intertropical Convergence Zone region toward the equator to 180°E. This feature is somewhat mirrored at the equator with the negative loadings outspreading from the coast of South American along curving trajectories toward the equator to about 170°E. Positive loadings are found north of PNG and surrounding New Caledonia. Its principal component (PC) is positively correlated with the EPEN index ($R = 0.71$) suggesting that the negative loadings on EOF1 show a decrease of biomass during EPEN events. Our result is consistent with Messié and Chavez (2012), who performed an EOF analysis on Chl-a as a proxy for biomass.

The second and third EOF modes (Figures S1c and S1e) explain 17.8% and 13.0% of the variance, respectively. Although both these EOF modes explain a total of 30.8% of the variance of biomass anomalies, a north test (North et al., 1982) verifies that the second and third EOF modes cannot be distinguished in a statistically significant way indicating that the signals are not well separated and cannot be physically explained. These limitations using the EOF procedure were also encountered by Singh et al. (2011) for sea surface salinity anomalies. Consequently, to effectively extract the dominant modes of variability, a combined regression-EOF (CR-EOF) analysis was performed on the biomass anomalies.

In performing the CR-EOF analysis, the CPEN index was first regressed onto the biomass anomalies. An EOF analysis was then carried out on the residuals of the regression values (residual is the variable minus the reconstructed variable that is derived from regression coefficients) to obtain the EP signature of ENSO (Singh et al., 2011). This method was applied to SST anomalies by Kao and Yu (2009) to separate EP and CP ENSO events. The first EOF explains 28.26% of the total variance in biomass anomalies (Figures S2a and S2b). The corresponding PC time series is positively correlated with N_{CT} ($R = 0.81$). The spatial pattern is similar to the EOF1 on the biomass anomalies in Figure S1a giving us confidence in the method applied to characterize El Niño types.

Using EPEN index as the regressor, the first EOF has a spatial structure of a large negative biomass pattern encompassed between 155°E–170°W, 5°S–5°N and explains 23.90% of the variance (Figures S2c and S2d). Positive biomass loadings are observed at the eastern outer edges of the tropical tongue and in the far northwestern Pacific. Its PC is positively correlated with N_{WP} ($R = 0.79$) indicating a decrease (increase) in biomass in the western-central (eastern) Pacific during CPEN events. The spatial feature is consistent with the second mode of EOF analysis of Chl-a in Messié and Chavez (2013).

4.2. AHC Analysis

The dominant patterns for both EPEN and CPEN events were obtained using the CR-EOF analysis. However, to better discriminate between El Niño types, due to possible limitations in using the EOF procedure (see Singh et al., 2011), we choose to use the agglomerative hierarchical clustering (AHC) technique to resolve El Niño types better.

Five clusters were identified using the AHC technique out of 124 monthly maps during 1997-2007 for the biomass anomalies. These five clusters represent intermediate CPEN, CPEN, LN, equatorial recovery, and EPEN conditions explaining 28.8%, 15.32%, 20.72%, 19.8%, and 15.32% of the variability, respectively (Figures 2a–2e). The extracted time series with cluster maps are shown in Figure 2f. Our cluster patterns for the biomass are similar to the five clusters identified by Radenac et al. (2012) but for Chl-a over the 1997-2010 period. We chose to keep the terminologies of the clusters similar as Radenac et al. (2012) for a consistent comparison.

Spatial patterns of Clusters 1 and 2 exhibit the intermediate CPEN and CPEN signals, respectively (Figures 2a and 2b). In cluster 1, the minimum biomass anomaly (less than -0.08 mg/m^3) is located between 150 and 160°E at the equator with curving trajectories of negative biomass anomalies extending toward the eastern Pacific along about 10°N-15°S. As the intermediate CPEN develops into CPEN (see Figure 2f), the negative core in the western Pacific grows and occupies a more extensive region [150°E-170°W, 5°N-5°S]. The two curving trajectories of negative biomass anomalies are replaced with positive anomalies in the

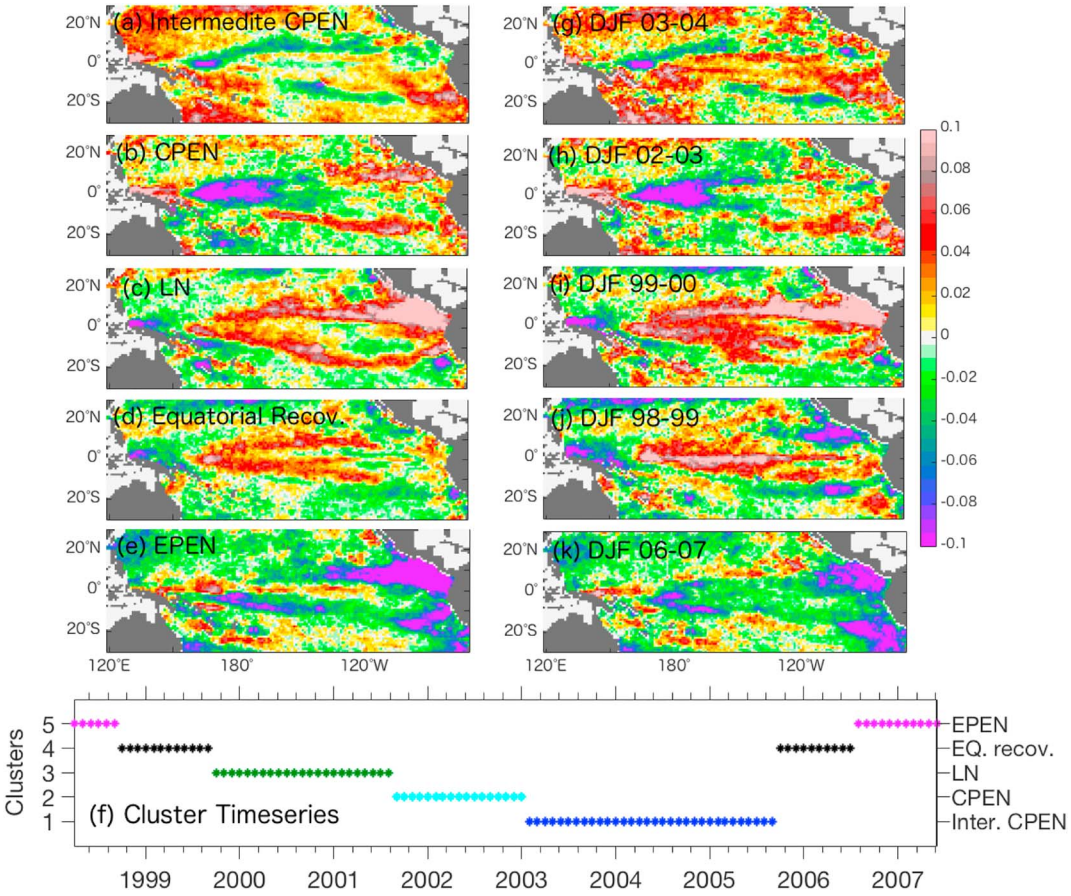

Figure 2. Phytoplankton biomass spatial maps for the (a) EPEN, (b) equatorial recovery conditions, (c) La Niña (LN), (d) intermediate Central Pacific El Niño (CPEN), (e) CPEN events, and the (f) cluster time series from agglomerative hierarchical clustering analysis. Three monthly December–February (DJF) composites of biomass anomalies for the years: (g) 2003-2004 intermediate CPEN, (h) 2002– 2003 CPEN, (i) 1999-2000 LN, (j) 1998–1999 equatorial recovery, and (k) 2006-2007 EPEN event. The units are mg C/m^3

eastern Pacific. The timing of biomass cluster 2 from AHC analysis are consistent with the previously documented CPEN events in 2002-2003 and 2004-2005 (Ashok et al., 2007; Kao & Yu, 2009; Kim & Yu, 2012; Kug et al., 2009; McPhaden et al., 2011; Radenac et al., 2012; Singh et al., 2011; Yeh et al., 2009), however noting that the 2004-2005 event is classified as an intermediate CPEN due to the magnitude of the biomass anomalies. The CPEN pattern from AHC is comparable to the spatial pattern obtained from the CR-EOF analysis (see Figure S2b).

Cluster 3 captures the spatial feature of LN, and the timing coincides with events in 1999-2000, and 2000-2001 (Figure 2c). The maximum biomass concentration is 10°N off the equator near the Central American coast, extending to the central Pacific Ocean between 0 and 5°N. The southern curving trajectory seen during cluster 1 and remain in cluster 3 albeit with dominantly positive biomass anomalies. Negative biomass anomalies are observed in the far western Pacific above PNG. During LN, the Eastern Pacific equatorial high biomass/Chl-a tongue is at its maximum extent due to the steepening of the basin-wide gradient of thermocline and nutricline across the region resulting in more upwelled nitrate and iron concentrations in the euphotic layer, preconditioning the waters for phytoplankton growth (Christian et al., 2001). Cluster 4 shows equatorial recovery with a spatial structure similar to that during LN (cluster 3) but with significantly reduced anomalies in the eastern Pacific.

Cluster 5 represents the EPEN event in 1997-1998 and 2006-2007 (Figure 2e). Cluster 5 spatial feature resembles the spatial feature in Figure S2a. A few studies characterized the 2006-2007 event as a CPEN event (Radenac et al., 2012, their Table 1).

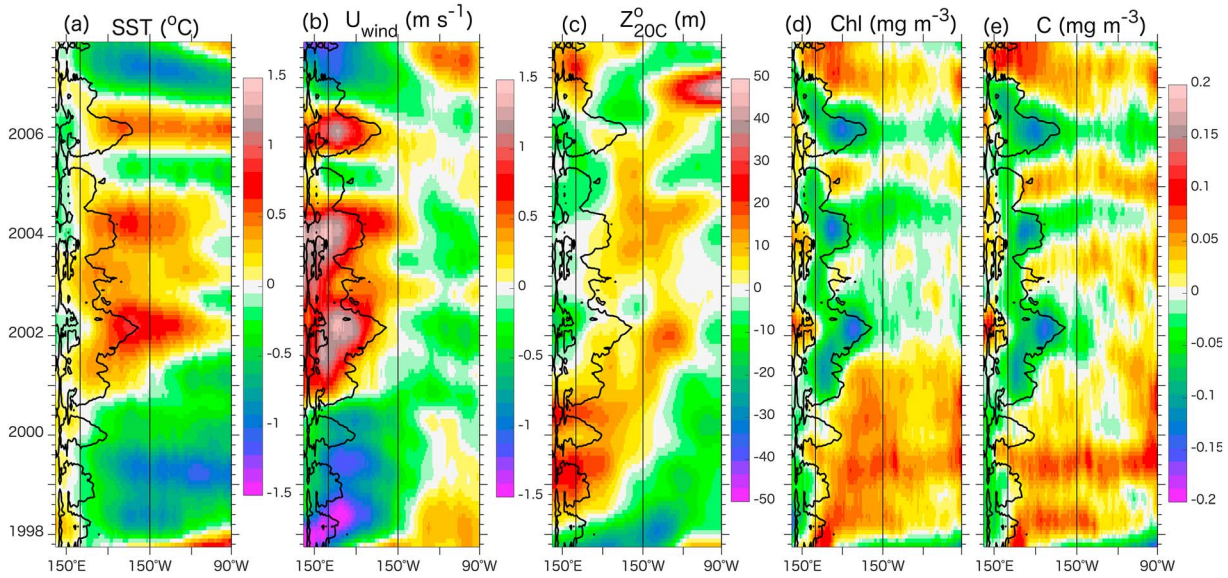

Figure 3. Time-longitude map for the (a) sea surface temperature (SST), (b) zonal wind speed (positive eastwards), (c) isothermal depth (positive deepens), (d) chlorophyll-a, and (e) biomass anomalies averaged between 5°S and 5°N. Note that we chose to show the surface chlorophyll-a thresholds lower than 0.1mg/m^3 as in Radenac et al. (2012) for comparison (in black contour lines). The vertical solid lines indicate the Niño3 (150°W, 90°W) and Niño4 (160°E, 150°W) boxes.

Representative examples of DJF (December to the following January) composites of biomass anomalies (Figures 2g–2k) give confidence that the clusters are not artifacts from the AHC analysis, rather they depict accurate instances biomass distribution. The subtle differences between the clusters and composites remind us of the uniqueness of each event.

5. Possible Drivers Responsible for EPEN and CPEN-Related Biomass Variations

5.1. Biomass in the Equatorial Region

Figure 3 illustrates the time-longitude distributions of the SST, zonal wind, thermocline (represented by the $Z_{20°C}$), Chl-a, and biomass anomalies averaged between 5°N and 5°S. Maximum positive SST anomalies are observed during El Niño events in 1997-1998 and 2002-2003, 2004-2005, and 2006-2007 (Figure 3a). During EPEN, anomalous westerly winds (Figure 3b) drive the strong anomalous eastward currents (not shown) advecting the nutrient poor (Figures 3d and 3e) warm pool waters eastward. As a result, tropical Pacific encounters long and persistent positive SST anomalies that enhances the vertical stratification and deepens the thermocline in the eastern tropics (Figure 3c) that weakens the upwelling. Overall, a flattened thermocline results over the basin (Chavez et al., 1998; Christian et al., 2001; Radenac et al., 2001; Stone et al., 1999; Strutton & Chavez, 2000; Turk et al., 2001).

The nitracline and equatorial undercurrent (EUC) deepening and weakened upwelling of cold nutrient-rich waters due to aforementioned process (nitrate-depleted surface layer; see Figure 3 schematics in Messié & Chavez, 2012) causes the decline in the phytoplankton growth in most of the tropical tongue region (Messié & Chavez, 2012; Radenac et al., 2012, and references therein). The primary driver of the anomalous biological changes is due to variations in the nutricline depth (depth where the nutrient concentration declines rapidly), decreasing nitrate content in the eastern Pacific during El Niño events and vice versa for LN events (Messié & Chavez, 2012). Deepening of the nutricline/thermocline or phytoplankton mixing length scales dilutes the phytoplankton in the surface ocean (Brody & Lozier, 2014) and thus allowing less sunlight to penetrate to the deeper water for photosynthesis. The lack of light in the deep water column limits the photosynthesis and phytoplankton growth, that is reflected in our biomass distribution (Figure 3e) during EPEN event. Messié and Chavez (2012) and Park et al. (2011) report similar changes but in Chl-a and also suggest that the light and nutrients drive the changes in the equatorial Pacific.

Studies have shown deeper ferricilne (depth at which iron concentration changes rapidly) than nutricline (Gordon et al., 1997) in the iron-limited equatorial Pacific (Martin et al., 1994). The ferricilne and

nutricline are coupled during El Niño when the ferricilne and EUC deepens (Barber et al., 1996; Johnson et al., 2002; Wilson & Adamec, 2001), thus reducing the vertical transfer of nutrient and iron concentration in the region (Chavez et al., 1999; Wang et al., 2005). Low supply of nitrate and iron suppresses the phytoplankton growth. Consequently, we observe Chl-a and biomass decrease during the 1997-1998 EPEN (Figures 3d and 3e, respectively), in agreement with previous work showing decreased Chl-a and PP during the same period (Behrenfeld et al., 2006; Christian et al., 2001; Messié & Radenac, 2006; Radenac et al., 2012). We also report similar declines in Chl-a in the ESA Ocean Color CCI product (Figure S3). A decrease in PP, ranging between 0.056 and 0.9 PgC/year has been reported in previous studies during the 1997-1998 EPEN event using different PP algorithms (Carr et al., 2006; Messié & Chavez, 2012; Racault et al., 2017).

Consistent with Kug et al. (2009) and Radenac et al. (2012), we report 1998-1999, 1999-2000, and 2000-2001 as LN years. Figure 3b shows an enhancement of the easterlies during LN events, driving strong westward currents (not shown), and pushing the warm-pool further west. In the central-eastern equatorial Pacific, the surface water is colder than normal (Figure 3a). The thermocline/nitracline tilt across the equatorial Pacific becomes steeper (deeper [shallower] in the west [east]). The intensified upwelling in the eastern Pacific is nutrient abundant, which preconditions the surface waters for phytoplankton growth and elevates the Chl-a and biomass concentrations (Figures 3d and 3e). The prolonged 1998-2001 LN event had exceptionally strong SST anomalies and was reported as an event that triggered significant phytoplankton blooms along the equatorial Pacific (Chavez et al., 1999; Martin et al., 1994; Messié & Radenac, 2006; Murtugudde et al., 1999; Ryan et al., 2002, 2006).

CPEN impacted the 2002-2005 period. The anomalous westerly winds are constricted to the western-central region extending the warm-pool to the central Pacific region only. The magnitude of the eastward extension of the warm-pool and the anomalous SST during EPEN is stronger than that of CPEN (Figure 3a). Radenac et al. (2012) suggested that zonal wind does not affect the eastern equatorial upwelling since its impact is confined within the central Pacific region. Therefore, nutrients are in excess in the eastern equatorial region, and the vertical movement of the thermocline will possibly not impact the biological activity. Instead, Radenac et al. (2012) proposed that the iron supply reduction due to EUC deepening terminates the phytoplankton growth, in agreement with Messié and Chavez (2012). In contrast, Messié & Chavez, 2013 using the second mode of the EOF analysis, which has similar spatial features as CPEN show that the Chl-a decrease in western-central region is due to an increase in barrier layer ("the layer between the mixed layer and the top of the thermocline"; Vialard & Delecluse, 1998) thickness and occurrence. The location and variations in barrier layer characteristics are governed by multiple mechanisms such as strengthened subtropical convergence due to intensified zonal winds, strong halocline between the warm-pool and cold tongue front and high rates of precipitation (Messié and Chavez (2013).

Furthermore, our characterization and response of biomass and physical parameters to CPEN and EPEN events over the 1997-2010 period are consistent with previous studies in the Equatorial Pacific (Gierach et al., 2012; Racault et al., 2017; Radenac et al., 2012; Turk et al., 2011). Notably, the composites reveal that the southern and northern edges of the negative biomass and Chl-a anomalies closely match the meridional extent of the anomalous eastward current. We observe that Chl-a and biomass are coupled during CP and EP ENSO between 10°N and 10°S. In the subtropics, Chl-a and biomass are decoupled mostly owing to photoacclimation (the ability of the phytoplankton to adjust to light levels; Siegel et al., 2013). In summary, a majority of the studies observed that decreases in tropical biological activity are governed by the disturbance in wind circulation that affects the vertical and horizontal transfer efficiency of nutrient content to the surface ocean (Ashok & Yamagata, 2009; Gierach et al., 2012; Messié & Chavez, 2012, 2013; Racault et al., 2017; Radenac et al., 2012).

5.2. Defining ENSO Metrics With Biomass

The distinctly different ENSO patterns observed using biomass anomalies allow us to define metrics to capture the different ENSO phases. We identify three most variable regions: the first region (R1) is delimited between 2.5°N-2.5°S and 147°E-170°W, the second region (R2) is between 4.5-12.5°N and 85-112°W, and the third region (R3) is between 13.5-20.5°S and 75-87°W. We empirically define the normalized biomass and Chl-a El Niño index (Figures S4a and S4b), using an empirical relationship as defined by the following equation:

$$\text{Biomass El Nino index} = [\text{PhytoA}]_{R1} - 0.3^{*}[\text{PhytoA}]_{R2} - 0.3^{*}[\text{PhytoA}]_{R3}$$

PhytoA is the area-weighted average biomass anomalies (or Chl-a anomalies) in the defined region boxes. The biomass and Chl-a El Niño index can distinguish between EPEN and CPEN events and has the high correlation of 0.71 and 0.92, respectively, with the Trans-Niño Index (TNI-defined as "the normalized difference between the normalized SST anomalies averaged in the Niño1+2 and Niño4 regions"; Trenberth & Stepaniak, 2001).

Since the biomass and Chl-a signatures are different during the El Niño and LN episodes, we define a biomass ENSO index using normalized sum between the area-weighted average biomass anomalies in the first two regions (R1+R2). The biomass ENSO index allows separating the warm and cold phase of ENSO (Figures S4a and S4b). Biomass and Chl-a ENSO indices are highly correlated with Southern Oscillation Index (SOI) of 0.77 and 0.81, respectively. The cluster time series fairly correspond with the biomass El Niño index and biomass ENSO index (Figure S4) that can be used to identify CPEN, EPEN, and LN events.

6. Summary

The objective of this research was to contrast EPEN and CPEN events in the tropical Pacific using satellite backscattering-derived phytoplankton biomass for the 1997-2007 period for the first time. Considering that the data from single SeaWiFs mission have several maps missing in year 2008, and the Kostadinov et al. (2010) product is not available for an extended period, we restricted our analysis from year 1997-2007. Using EOF, CR-EOF, and AHC on biomass, we showed that EPEN events in biomass are evident in 1997-1998 and 2006-2007, intermediate CPEN and CPEN events between 2002 and 2005, and LN events in 1999-2001. We report similar drivers for biomass and Chl-a, as indicated by Radenac et al. (2012) for Chl-a only. During the CPEN events, changes in the vertical supply of iron concentrations due to EUC vertical displacement (Radenac et al., 2012) and the strength of subtropical gyres (Messié & Chavez, 2013) drawdowns the biological activity in the iron-limited region. During EPEN, anomalous westerly winds drive strong anomalous eastward currents. The nutrient-deprived western warm waters extend to 130°W reducing the upwelling and deepening the nitracline and EUC. Reduced surface nutrients reduce the biological activity, lowering the biomass and Chl-a concentrations. Each EPEN and CPEN event will impact the phytoplankton abundance differently, affecting the fish abundance and thus fisheries industries (Racault et al., 2017).

This study focused on using satellite derived ocean-color products to understand the variability of biomass on ENSO timescales. We also acknowledge the biases and uncertainties present in the Kostadinov et al. (2016) biomass due to the assumptions and sensitivity of the carbon product inputs in the algorithm. One of the quantified partial uncertainties is higher estimate for the total phytoplankton C biomass in the productive regions, for example, equatorial upwelling region and high latitudes. The resulting is due to the large sources of error in inputs (e.g., number of particles and PSD) due to the natural variability of the complex index of refraction and the maximum diameter of the particles considered and uncertainties in the coefficients used in algorithms.

Possible mechanisms to explain biomass distribution have been highlighted. What remains to be investigated is how the frequency of different ENSO types and their amplitude affect the long-term biomass trend. It should be noted however that a clean separation is required to distinguish the natural forcing's from anthropogenic forcing's (Henson et al., 2010). Another interesting question to be addressed is how the different ENSO types affect the phytoplankton biomass in the subpolar regions.

Acknowledgments
Kostadinov et al. (2009, 2010, 2016) products are available at https://doi.pangaea.de/10.1594/PANGAEA.859005.

References

Ashok, K., Behera, S. K., Rao, S. A., Weng, H., & Yamagata, T. (2007). El Niño Modoki and its possible teleconnection. *Journal of Geophysical Research*, *112*, C11007. https://doi.org/10.1029/2006JC003798

Ashok, K., & Yamagata, T. (2009). The El Niño with a difference. *Nature*, *461*(7263), 481–484. https://doi.org/10.1038/461481a

Barber, R. T., Sanderson, M. P., Lindley, S. T., Chai, F., Newton, J., Trees, C. C., et al. (1996). Primary productivity and its regulation in the equatorial Pacific during and following the 1991–1992 El Niño. *Deep Sea Research Part II: Topical Studies in Oceanography*, *43*(4-6), 933–969. https://doi.org/10.1016/0967-0645(96)00035-5

Behrenfeld, M. J., Boss, E., Siegel, D. A., & Shea, D. M. (2005). Carbon-based ocean productivity and phytoplankton physiology from space. *Global Biogeochemical Cycles*, *19*, GB1006. https://doi.org/10.1029/2004GB002299

Behrenfeld, M. J., O'Malley, R. T., Siegel, D. A., McClain, C. R., Sarmiento, J. L., Feldman, G. C., et al. (2006). Climate-driven trends in contemporary ocean productivity. *Nature*, *444*(7120), 752–755. https://doi.org/10.1038/nature05317

Berrisford, P., Dee, D., Poli, P., Brugge, R., Fielding, K., Fuentes, M., et al. (2011). The ERA-Interim archive Version 2.0. ERA Report Series 1, ECMWF, Shinfield Park, Reading, UK, 13177.

Bonjean, F., & Lagerloef, G. S. E. (2002). Diagnostic model and analysis of the surface currents in the tropical Pacific Ocean. *Journal of Physical Oceanography*, *32*(10), 2938–2954. https://doi.org/10.1175/1520-0485(2002)032<2938:DMAAOT>2.0.CO;2

Brody, S. R., & Lozier, M. S. (2014). Changes in dominant mixing length scales as a driver of subpolar phytoplankton bloom initiation in the North Atlantic. *Geophysical Research Letters*, *41*, 3197–3203. https://doi.org/10.1002/2014GL059707

Carr, M.-E., Friedrichs, M. A. M., Schmeltz, M., Noguchi Aita, M., Antoine, D., Arrigo, K. R., et al. (2006). A comparison of global estimates of marine primary production from ocean color. *Deep Sea Research Part II: Topical Studies in Oceanography*, *53*(5-7), 741–770. https://doi.org/10.1016/j.dsr2.2006.01.028

Chavez, F. P., Strutton, P. G., Friederich, G. E., Feely, R. A., Feldman, G. C., Foley, D. G., & McPhaden, M. J. (1999). Biological and chemical response of the equatorial Pacific Ocean to the 1997-98 El Niño. *Science*, *286*(5447), 2126–2131. https://doi.org/10.1126/science.286.5447.2126

Chavez, F. P., Strutton, P. G., & McPhaden, M. J. (1998). Biological-physical coupling in the Central Equatorial Pacific during the onset of the 1997–98 El Niño. *Geophysical Research Letters*, *25*(19), 3543–3546. https://doi.org/10.1029/98GL02729

Christian, J. R., Verschell, M. A., Murtugudde, R., Busalacchi, A. J., & McClain, C. R. (2001). Biogeochemical modelling of the tropical Pacific Ocean. I: Seasonal and interannual variability. *Deep Sea Research Part II: Topical Studies in Oceanography*, *49*(1–3), 509–543. https://doi.org/10.1016/S0967-0645(01)00110-2

Feng, J., & Li, J. (2011). Influence of El Niño Modoki on spring rainfall over south China. *Journal of Geophysical Research*, *116*, D13102. https://doi.org/10.1029/2010JD015160

Gierach, M. M., Lee, T., Turk, D., & McPhaden, M. J. (2012). Biological response to the 1997-98 and 2009-10 El Niño events in the equatorial Pacific Ocean. *Geophysical Research Letters*, *39*, L10602. https://doi.org/10.1029/2012GL051103

Gordon, H. R., & Morel, A. (1983). *Remote Assessment of Ocean Color for Interpretation of Satellite Visible Imagery: A Review* (p. 44). New York: Springer.

Gordon, R. M., Coale, K. H., & Johnson, K. S. (1997). Iron distributions in the equatorial Pacific: Implications for new production. *Limnology and Oceanography*, *42*(3), 419–431. https://doi.org/10.4319/lo.1997.42.3.0419

Henson, S. A., Sarmiento, J. L., Dunne, J. P., Bopp, L., Lima, I., Doney, S. C., et al. (2010). Detection of anthropogenic climate change in satellite records of ocean chlorophyll and productivity. *Biogeosciences*, *7*(2), 621–640. https://doi.org/10.5194/bg-7-621-2010

Johnson, G. C., Sloyan, B. M., Kessler, W. S., & McTaggart, K. E. (2002). Direct measurements of upper ocean currents and water properties across the tropical Pacific during the 1990s. *Progress in Oceanography*, *52*(1), 31–61. https://doi.org/10.1016/S0079-6611(02)00021-6

Kao, H.-Y., & Yu, J.-Y. (2009). Contrasting Eastern-Pacific and Central-Pacific Types of ENSO. *Journal of Climate*, *22*(3), 615–632. https://doi.org/10.1175/2008jcli2309.1

Kim, S. T., & Yu, J.-Y. (2012). The two types of ENSO in CMIP5 models. *Geophysical Research Letters*, *39*, L11704. https://doi.org/10.1029/2012GL052006

Kostadinov, T. S., Cabré, A., Vedantham, H., Marinov, I., Bracher, A., Brewin, R. J. W., et al. (2017). Inter-comparison of phytoplankton functional type phenology metrics derived from ocean color algorithms and Earth System Models. *Remote Sensing of Environment*, *190*, 162–177. https://doi.org/10.1016/j.rse.2016.11.014

Kostadinov, T. S., Milutinović, S., Marinov, I., & Cabré, A. (2016). Carbon-based phytoplankton size classes retrieved via ocean color estimates of the particle size distribution. *Ocean Science*, *12*(2), 561–575. https://doi.org/10.5194/os-12-561-2016

Kostadinov, T. S., Siegel, D. A., & Maritorena, S. (2009). Retrieval of the particle size distribution from satellite ocean color observations. *Journal of Geophysical Research*, *114*, C09015. https://doi.org/10.1029/2009JC005303

Kostadinov, T. S., Siegel, D. A., & Maritorena, S. (2010). Global variability of phytoplankton functional types from space: Assessment via the particle size distribution. *Biogeosciences*, *7*(10), 3239–3257. https://doi.org/10.5194/bg-7-3239-2010

Kug, J.-S., Jin, F.-F., & An, S.-I. (2009). Two types of El Niño events: Cold tongue El Niño and Warm Pool El Niño. *Journal of Climate*, *22*(6), 1499–1515. https://doi.org/10.1175/2008jcli2624.1

Larkin, N. K., & Harrison, D. E. (2005a). On the definition of El Niño and associated seasonal average U.S. weather anomalies. *Geophysical Research Letters*, *32*, L13705. https://doi.org/10.1029/2005GL022738

Larkin, N. K., & Harrison, D. E. (2005b). Global seasonal temperature and precipitation anomalies during El Niño autumn and winter. *Geophysical Research Letters*, *32*, L16705. https://doi.org/10.1029/2005GL022860

Lundry, M. R., Barber, R. T., Bidare, R. R., Chai, F., Coale, K. H., Dam, H. G., et al. (2003). Iron and grazing constraints on primary production in the central equatorial Pacific: An EqPac synthesis. *Limnology and Oceanography*, *42*(3), 405–418. https://doi.org/10.4319/lo.1997.42.3.0405

Martin, J. H., Coale, K. H., Johnson, K. S., Fitzwater, S. E., Gordon, R. M., Tanner, S. J., et al. (1994). Testing the iron hypothesis in ecosystems of the equatorial Pacific Ocean. *Nature*, *371*(6493), 123–129. https://doi.org/10.1038/371123a0

McPhaden, M. J., Busalacchi, A. J., Cheney, R., Donguy, J.-R., Gage, K. S., Halpern, D., et al. (1998). The tropical ocean-global atmosphere observing system: A decade of progress. *Journal of Geophysical Research*, *103*(C7), 14,169-14,240. https://doi.org/10.1029/97JC02906

McPhaden, M. J., Lee, T., & McClurg, D. (2011). El Niño and its relationship to changing background conditions in the tropical Pacific Ocean. *Geophysical Research Letters*, *38*, L15709. https://doi.org/10.1029/2011GL048275

Menden-Deuer, S., & Lessard, E. J. (2000). Carbon to volume relationships for dinoflagellates, diatoms, and other protist plankton. *Limnology and Oceanography*, *45*(3), 569–579. https://doi.org/10.4319/lo.2000.45.3.0569

Messié, M., & Chavez, F. P. (2012). A global analysis of ENSO synchrony: The oceans' biological response to physical forcing. *Journal of Geophysical Research*, *117*, C09001. https://doi.org/10.1029/2012JC007938

Messié, M., & Chavez, F. P. (2013). Physical-biological synchrony in the global ocean associated with recent variability in the central and western equatorial Pacific. *Journal of Geophysical Research: Oceans*, *118*, 3782–3794. https://doi.org/10.1002/jgrc.20278

Messié, M., & Radenac, M.-H. (2006). Seasonal variability of the surface chlorophyll in the western tropical Pacific from SeaWiFS data. *Deep Sea Research Part I: Oceanographic Research Papers*, *53*(10), 1581–1600. https://doi.org/10.1016/j.dsr.2006.06.007

Mobley, C. D., Sundman, L. K., & Boss, E. (2002). Phase function effects on oceanic light fields. *Applied Optics*, *41*(6), 1035–1050. https://doi.org/10.1364/AO.41.001035

Mouw, C. B., Hardman-Montford, N., Alvain, S., Bracher, A., Brewin, R., Bricaud, A., et al. (2017). A consumer's guide to satellite remote sensing of multiple phytoplankton groups in the global ocean. *Frontiers in Marine Science*, *4*, 41. https://doi.org/10.3389/fmars.2017.00041

Murtugudde, R. G., Signorini, S. R., Christian, J. R., Busalacchi, A. J., McClain, C. R., & Picaut, J. (1999). Ocean color variability of the tropical Indo-Pacific basin observed by SeaWiFS during 1997–1998. *Journal of Geophysical Research*, *104*(C8), 18,351–18,366. https://doi.org/10.1029/1999JC900135

North, G. R., Bell, T. L., Cahalan, R. F., & Moeng, F. J. (1982). Sampling errors in the estimation of empirical orthogonal functions. *Monthly Weather Review*, *110*, 699–706.

Park, J.-Y., Kug, J.-S., Park, J., Yeh, S.-W., & Jang, C. J. (2011). Variability of chlorophyll associated with El Niño–Southern Oscillation and its possible biological feedback in the equatorial Pacific. *Journal of Geophysical Research*, *116*, C10001. https://doi.org/10.1029/2011JC007056

Racault, M.-F., Sathyendranath, S., Brewin, R. J. W., Raitsos, D. E., Jackson, T., & Platt, T. (2017). Impact of El Niño variability on oceanic phytoplankton. *Frontiers in Marine Science*, *4*, 133. https://doi.org/10.3389/fmars.2017.00133

Racault, M. F., Sathyendranath, S., Menon, N., & Platt, T. (2016). Phenological responses to ENSO in the global oceans. *Surveys in Geophysics*, *38*(1), 277–293. https://doi.org/10.1007/s10712-016-9391-1

Radenac, M.-H., Léger, F., Singh, A., & Delcroix, T. (2012). Sea surface chlorophyll signature in the tropical Pacific during eastern and central Pacific ENSO events. *Journal of Geophysical Research*, *117*, C04007. https://doi.org/10.1029/2011JC007841

Radenac, M. H., Menkes, C., Vialard, J., Moulin, C., Dandonneau, Y., Delcroix, T., et al. (2001). Modeled and observed impacts of the 1997–1998 El Niño on nitrate and new production in the equatorial Pacific. *Journal of Geophysical Research*, *106*(C11), 26,879–26,898. https://doi.org/10.1029/2000JC000546

Ren, H.-L., & Jin, F.-F. (2011). Niño indices for two types of ENSO. *Geophysical Research Letters*, *38*, L04704. https://doi.org/10.1029/2010GL046031

Ryan, J. P., Polito, P. S., Strutton, P. G., & Chavez, F. P. (2002). Unusual large-scale phytoplankton blooms in the equatorial Pacific. *Progress in Oceanography*, *55*(3-4), 263–285. https://doi.org/10.1016/S0079-6611(02)00137-4

Ryan, J. P., Ueki, I., Chao, Y., Zhang, H., Polito, P. S., & Chavez, F. P. (2006). Western Pacific modulation of large phytoplankton blooms in the central and eastern equatorial Pacific. *Journal of Geophysical Research*, *111*, G02013. https://doi.org/10.1029/2005JG000084

Sathyendranath, S., & Platt, T. (1989). Remote sensing of ocean chlorophyll: consequence of nonuniform pigment profile. *Applied Optics*, *28*(3), 490–495. https://doi.org/10.1364/AO.28.000490

Siegel, D. A., Behrenfeld, M. J., Maritorena, S., McClain, C. R., Antoine, D., Bailey, S. W., et al. (2013). Regional to global assessments of phytoplankton dynamics from the SeaWiFS mission. *Remote Sensing of Environment*, *135*, 77–91. https://doi.org/10.1016/j.rse.2013.03.025

Singh, A., Delcroix, T., & Cravatte, S. (2011). Contrasting the flavors of El Niño-Southern Oscillation using sea surface salinity observations. *Journal of Geophysical Research*, *116*, C06016. https://doi.org/10.1029/2010JC006862

Stone, L., Rajagopalan, B., Bhasin, H., & Loya, Y. (1999). Mass Coral Reef Bleaching: A Recent Outcome of Increased El Niño Activity? *Ecology Letters*, *2*(5), 325–330. https://doi.org/10.1046/j.1461-0248.1999.00092.x

Stramski, D., & Kiefer, D. A. (1991). Light scattering by microorganisms in the open ocean. *Progress in Oceanography*, *28*(4), 343–383. https://doi.org/10.1016/0079-6611(91)90032-H

Strutton, P. G., & Chavez, F. P. (2000). Primary productivity in the equatorial Pacific during the 1997–1998 El Niño. *Journal of Geophysical Research*, *105*(C11), 26,089–26,101. https://doi.org/10.1029/1999JC000056

Trenberth, K. E., & Stepaniak, D. P. (2001). Indices of El Niño Evolution. *Journal of Climate*, *14*(8), 1697–1701. https://doi.org/10.1175/1520-0442(2001)014<1697:LIOENO>2.0.CO;2

Turk, D., McPhaden, M. J., Busalacchi, A. J., & Lewis, M. R. (2001). Remotely Sensed Biological Production in the Equatorial Pacific. *Science*, *293*(5529), 471–474. https://doi.org/10.1126/science.1056449

Turk, D., Meinen, C. S., Antoine, D., McPhaden, M. J., & Lewis, M. R. (2011). Implications of changing El Niño patterns for biological dynamics in the equatorial Pacific Ocean. *Geophysical Research Letters*, *38*, L23603. https://doi.org/10.1029/2011GL049674

Vialard, J., & Delecluse, P. (1998). An OGCM study for the TOGA decade. Part II: Barrier layer formation and variability. *Journal of Physical Oceanography*, *28*(6), 1089–1106. https://doi.org/10.1175/1520-0485(1998)028<1089%3AAOSFTT>2.0.CO%3B2

Wang, C., & Weisberg, R. H. (2000). The 1997–98 El Niño evolution relative to previous El Niño events. *Journal of Climate*, *13*(2), 488–501. https://doi.org/10.1175/1520-0442(2000)013<0488:TENOER>2.0.CO;2

Wang, X., Christian, J. R., Murtugudde, R., & Busalacchi, A. J. (2005). Ecosystem dynamics and export production in the central and eastern equatorial Pacific: A modeling study of impact of ENSO. *Geophysical Research Letters*, *32*, L02608. https://doi.org/10.1029/2004GL021538

Wilson, C., & Adamec, D. (2001). Correlations between surface chlorophyll and sea surface height in the tropical Pacific during the 1997-1999 El Niño-Southern Oscillation event. *Journal of Geophysical Research*, *106*(C12), 31,175–31,188. https://doi.org/10.1029/2000JC000724

Yeh, S. W., Kug, J. S., Dewitte, B., Kwon, M. H., Kirtman, B. P., & Jin, F. F. (2009). El Niño in a changing climate. *Nature*, *461*(7263), 511–514. https://doi.org/10.1038/nature08316

Yu, J.-Y., & Kim, S. T. (2010). Identification of Central-Pacific and Eastern-Pacific types of ENSO in CMIP3 models. *Geophysical Research Letters*, *37*, L15705. https://doi.org/10.1029/2010GL044082

Zhang, W., Jin, F.-F., Li, J., & Ren, H.-L. (2011). Contrasting Impacts of Two-Type El Niño over the Western North Pacific during Boreal Autumn. *Journal of the Meteorological Society of Japan. Series II*, *89*(5), 563–569. https://doi.org/10.2151/jmsj.2011-510

References From the Supporting Information

Steinmetz, F., Deschamps, P.-Y., & Ramon, D. (2011). Atmospheric correction in presence of sun glint: application to MERIS. *Optics Express*, *19*(10), 9783–9800. https://doi.org/10.1364/OE.19.009783